A Tough Metal-Coordinated Elastomer: A Fatigue-Resistant, Notch-Insensitive Material with an Excellent Self-Healing Capacity

Gai, Guangjie ; Liu, Libin; Li, Cheng-Hui; Bose, Ranjita; Li, Dong ; Guo, Ning; Kong, Biao

Published in:
ChemPlusChem

DOI:
10.1002/cplu.201900095

Publication date:
2019

ChemPubSoc Europe

DOI: 10.1002/cplu.201900095

CHEMPLUSCHEM Full Papers

A Tough Metal-Coordinated Elastomer: A Fatigue-Resistant, Notch-Insensitive Material with an Excellent Self-Healing Capacity

Guangjie Gai,[a] Libin Liu,*[a] Cheng-Hui Li,[b] Ranjita K. Bose,[c] Dong Li,[a] Ning Guo,[a] and Biao Kong[d]

Self-healing materials can prolong device life, but their relatively weak mechanical strength limits their applications. Introducing tunable metal-ligand interactions into self-healing systems can improve their mechanical strength. However, applying this concept to solid elastomers is a challenge. To address this need, polyurethane-containing metal complexes were fabricated by introduction of a pyridine-containing ligand into polyurethane, and subsequent coordination with Fe^{2+}. The strong reversible coordination bond provides mechanical strength and self-healing ability. By optimizing the monomer ratio and Fe^{2+} content, the resulting complex possesses a very high tensile strength of 4.6 MPa at strain of around 498% and a high Young's modulus (3.2 MPa). Importantly, the metal complex exhibits an extremely high self-healing efficiency of approximately 96% of tensile strength at room temperature and around 30% at 5 °C. The complex is notch-insensitive and the fracture energy is 76186 J/m^2, which is among the highest reported values for self-healing systems.

Introduction

In nature, organisms have the self-healing ability to repair damage spontaneously and thus prolonging their lifespan. In a similar way, synthetic self-healable polymers are able to repair themselves and recover functionalities after being mechanically damaged.[1] In such materials, the use of vascular or capsule-based system for storage and release of healing agents is employed (also called extrinsic healing method).[2] This kind of healing approach depends on the utilized healing agents, where exhaustion of reagents will lead to repair termination. An alternative (also called intrinsic healing method) is the utilization of dynamic covalent bonds[3](e.g. Diels-Alder reaction, disulfide bond) or noncovalent interactions (e.g. ionic interactions,[4] hydrogen bonding,[5] π-π interactions,[6] host-guest interactions,[7] metal-ligand-interactions[8]), which provide an efficient path toward autonomous, repeatable self-healing. Although significant progress has been achieved on the self-healing materials, design and fabrication of intrinsic self-healable materials with high self-healing efficiency under mild conditions as well as robust mechanical properties remain an ongoing challenge.

Metal-ligand interaction, as one of reversible noncovalent interactions, is attractive in self-healing systems because it can provide a certain mechanical property for the composite due to the moderate bonding energy (50–200 kJ/mol) between the low hydrogen bonding energy (25–40 kJ/mol) and the high covalent bonding energy (greater than 350 kJ/mol). Up to now, a vast range of accessible ligands and metal ions are used in self-healing systems.[9] For example, Weder and co-workers reported optically healable supramolecular polymers by using 2,6-bis(19-methylbenzimidazolyl)pyridine as ligands.[10] The resulting supramolecular complex could heal the damage at high temperature of 220 °C or upon exposure to UV light. Weng and coworker fabricated different healable metallo-supramolecular materials by incorporating 2,6-bis(1,2,3-triazol-4-yl)pyridine ligands into the polymer backbone.[11] Gong et al. reported a superior mechanical metallo-supramolecular polymer with multi-stimuli responsive self-healing properties.[12] Most of these metal coordinated complexes can heal themselves basically under external conditions such as light, heating or certain solvents. Other examples via metal-ligands interactions can heal at room temperature without any stimuli,[13] but these systems usually have weak mechanical strengths and low fracture energies (typically at ~100 J/m^2 or less).[14] Thus, developing metal-coordinated polymeric materials with superior mechanical properties that can be healed in ambient conditions still remains largely unexplored.

[a] G. Gai, Prof. Dr. L. Liu, D. Li, Dr. N. Guo
Institute of Advanced Energy Materials and Chemistry
School of Chemistry and Pharmaceutical Engineering
State Key Laboratory of Biobased Material and Green Papermaking
Qilu University of Technology (Shandong Academy of Sciences)
Jinan 250353 (P. R. China)
E-mail: lbliu@qlu.edu.cn
[b] Dr. C.-H. Li
State Key Laboratory of Coordination Chemistry
School of Chemistry and Chemical Engineering
Nanjing University
Nanjing 210093 (P. R. China)
[c] Dr. R. K. Bose
Engineering and Technology Institute Groningen (ENTEG)
University of Groningen
Nijenborgh 4, 9747AG Groningen (The Netherlands)
[d] Dr. B. Kong
Department of Chemistry
Shanghai Key Lab of Molecular Catalysis and Innovative MaterialsiChEM
Fudan University
Shanghai 200433 (P. R. China)

Supporting information for this article is available on the WWW under https://doi.org/10.1002/cplu.201900095

Because metal-ligand interactions can have single, double or multiple coordination sites and the binding strengths are tunable, the resulting metal complexes usually have a variety of topological structures.[15] By controlling the types of ligands and metal ions, it is possible to achieve the reversible networks without external stimuli at room temperature. Indeed, Guan and coworker demonstrated a self-healing polymer by choosing a highly dynamic Zn^{2+}-imidazole as the healing motif in a hard/soft two-phase brush copolymer system, which exhibits super self-healing ability at room temperature without any intervention.[16]

Considering the strong coordination ability of tripyridine/dipyridine and metal ion,[17] in this work, a simple mono-pyridine group containing diol (PY) as the ligand was designed and introduced into polyurethane (PU) (Figure 1a). The resulting

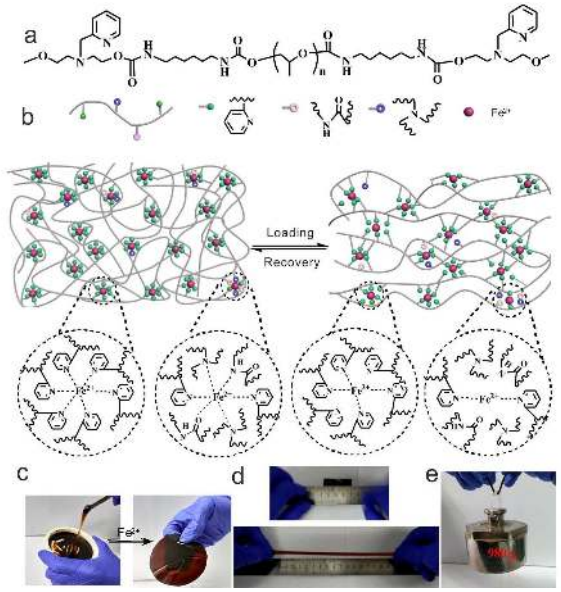

Figure 1. (a) Representative PU structure fabricated by hexamethylene diisocyanate (HDI), poly(propylene glycol) (PPG) and PY. (b) Schematic metal-coordinated PU complex and a proposed coordination geometry in the process of loading and recovery. (c) Photographs of a pristine PU and corresponding Fe^{2+}-coordinated PU. (d) Photographs of a highly stretched complex. (e) Photographs of loading 0.98 kg by a complex rod (2.2 mm in diameter).

metal-PU complexes possess both super self-healing ability and high mechanical strength through multiple coordination interactions between polyurethane backbone and metal ions (Fe^{2+}). The coordination bonds between pyridine group and Fe^{2+} function as strong cross-linkers, providing strength of the complex. The rupture and reconstruction of Fe^{2+}-PY bond and the weak coordination bonds between the amide and Fe^{2+} will dissipate the strain energy, thus leading to the self-healing ability (Figure 1b). As a result, the coordination density of available metal-ligand interactions can be tuned by PY contents and the molar ratio of the different segments. The resulting metal-coordinated PU exhibits super mechanical properties, such as high tensile strength (up to 4.64 MPa), high elongation (~497.5%) at strain rate of 100 mm/min, and high Young's modulus (~3.2 MPa) and. Importantly, the metal-complex exhibits outstanding self-healing efficiency of ~96% of tensile strength at room temperature and ~30% at low temperature of 5 °C. More importantly, the complex is notch-insensitive and the fracture energy is ~76186 J/m^2, which is among the highest values in the reported self-healing polymeric materials.

Results and Discussion

For fabrication of polyurethane, pyridine-containing diol (PY) was first synthesized as shown in Scheme S1 and experimental section. The coordination between PY and Fe^{2+} was proved by the new peak centered at 325 nm, which may be caused by charge-transfer electronic transfer from metal to ligand (Figure S2a). When the molar ratio of metal ion to ligand (Fe^{2+}:PY) reaches to 1:6, the peak is saturated (Figure S2b), which is in accordance with octahedral geometry between Fe^{2+} and bipyridine.[17b] The PU was synthesized by condensation reaction by using HDI and PPG and subsequent PY as chain extender (see experimental section). The obtained PU is weak and sticky. After addition of $FeSO_4$ in PU methanol solution, the UV-vis spectra revealed the similar changes of the absorption peaks, which suggested that the Fe^{2+} was coordinated with PY in the PU backbone (Figure S3). In addition, FTIR spectra revealed that a characteristic absorption peak at 1594 cm^{-1} was seen on a spectrum of pure PY, indicating C=N vibration modes on free pyridine rings. After addition of Fe^{2+}, a new shoulder appears at 1605 cm^{-1}, suggesting successful coordination of PY and Fe^{2+}. When the PY was incorporated PU, after coordination the peak slightly shifts to 1607 cm^{-1}[19] (Figure S4). The metal-coordinated PU solutions were poured into a Teflon mold. After evaporation of solvent, the film was obtained, which is strong and stiff and can be self-standing films (Figure 1c). The complex film can be stretched by hand to a great extent (Figure 1d). After heating at 85 °C for a few minutes, the complex film was rolled into a rod with cylinder shape. A metal-coordinated PU rod with a diameter of 2.2 mm can load 0.98 kg of weight (Figure 1e). The excellent mechanical performance of the metal-coordinated PUs is related to the segment ratio and the density of coordination bonds. Therefore, to optimize the appropriate segment ratio, different PUs (abbreviated $HDI_xPPG_yPY_z$, where x, y, z refer to the molar ratio of HDI, PPG and PY, PPG = 400 g/mol) coordinated with different content of $FeSO_4$ (Fe^{2+}:PY = 1:4, 1:6, 1:8) were synthesized. The rheological properties of all complexes are shown in Figure 2a–b and Figure S5, S6. The linear viscoelasticity regions were first determined by plotting the storage modulus (G′, representing an elastic response) and loss modulus (G″, representing a viscous response) against oscillatory strain in the range of 0.1~100% at 10 rad/s (Figure 2a and Figure S5a, S6a). Therefore, to ensure the linear viscoelasticity and sufficient sensitivity, a strain of 1% was selected to measure viscoelasticity. For all pristine PUs, the G″ is higher than G′, which indicates the liquid behavior. After coordination with Fe^{2+}, the G′ increases and is higher than G″, indicating the solid behavior. It should be noted that for all PU/Fe^{2+} complexes, the complexes with Fe^{2+}:PY ratio of 1:6

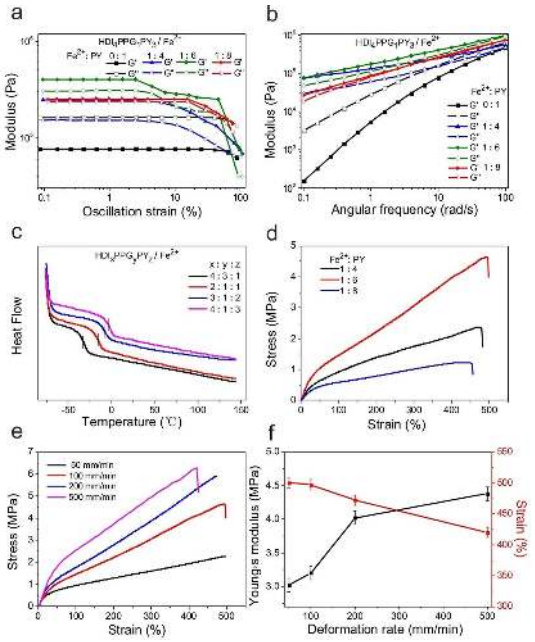

Figure 2. Rheological properties of $HDI_4PPG_1PY_3/Fe^{2+}$ complex at different ratio of Fe^{2+} and PY. Storage modulus (G′, filled symbols) and loss modulus (G″, empty symbols) are plotted against oscillation strain (a) and angular frequency (b). (c) DSC data of different PU/Fe^{2+} complexes at Fe^{2+} and PY ratio of 1:6. (d) Stress-strain curves of the $HDI_4PPG_1PY_3/Fe^{2+}$ complex at Fe^{2+} and PY ratio of 1:4, 1:6, and 1:8, respectively. (e) Tensile behavior of the $HDI_4PPG_1PY_3/Fe^{2+}$ complex (Fe^{2+}:PY = 1:6) under different deformation rates in the range of 50–500 mm/min. (f) Young's modulus and tensile strain of the $HDI_4PPG_1PY_3/Fe^{2+}$ complex (Fe^{2+}:PY = 1:6) as a function of deformation rate.

exhibit higher modulus compared to the complexes with metal: ligand ratio of 1:4 and 1:8, implying that the appropriate metal-ligand ratio of Fe^{2+}:PY is 1:6, which is consistent with the UV-vis titrations experiments. The PU/Fe^{2+} complex with higher metal-ligand ratio of 1:8 exhibits lower mechanical strength, which may be due to that the too many free ligands make the whole system more dynamic, resulting in a lower modulus of the complexes.[20] We also compared the effect of the molecular weight of PPG on the viscoelasticity. As shown in Figure S7, the modulus of the complex by using low molecular weight of PPG (400 g/mol) is higher than that of the complex by using high molecular weight of PPG (1000 g/mol). Considering that our aim is to fabricate polymeric materials with high modulus and high self-healing efficiency, PPG with molecular weight of 400 g/mol is used.

Since the increase in the PY contents of the polyurethane results in more coordination sites, the glass transition temperature (T_g) values of the complexes also increases as the PY contents increases as confirmed by their differential scanning calorimetry (DSC) measurements. In specific, at Fe^{2+}:PY molar ratio of 1:6, the $HDI_4PPG_3PY_1/Fe^{2+}$ complex with the lowest PY contents has the lowest T_g of −32 °C, while the T_g of $HDI_2PPG_1PY_1/Fe^{2+}$ and $HDI_3PPG_1PY_2/Fe^{2+}$ complexes increase to −16 °C and −9 °C, respectively. For $HDI_4PPG_1PY_3/Fe^{2+}$ complex with highest PY contents, T_g reaches to the highest value of −5 °C. In addition, to clarify the change of T_g upon varying metal concentration, $HDI_4PPG_1PY_3/Fe^{2+}$ complex with different amount of metal ions is also measured (Figure S8). When the molar ratio of Fe^{2+}:PY is 0:1, 1:8, 1:6, 1:4, correspondingly, the glass transition temperature is −13, −8, −5, −6 °C, respectively. This indicates that the T_g increases with increasing in the Fe^{2+} contents. However, excess Fe^{2+} results in decrease in the T_g. The highest T_g of $HDI_4PPG_1PY_3/Fe^{2+}$ complex with the molar ratio of Fe^{2+}:PY at 1:6 indicates the highest mechanical strength, which is consist with the results measured in rheological and tensile tests. It should be noted that all the complexes possess T_g values of below room temperature, suggesting that these complexes are in the viscoelastic state and they have potential for self-healing at room temperature. The different metal-ligand ratio of the complex also affects the mechanical strength. For example, the stress-strain curves in the case of $HDI_4PPG_1PY_3/Fe^{2+}$ demonstrated that the complex with metal-ligand ratio of 1:4 possesses stress of 2.36 MPa at strain of ~481.5%, and the complex with metal-ligand ratio of 1:8 possesses stress of 1.23 MPa, while the complex with Fe^{2+}:PY of 1:6 shows the highest stress of 4.64 MPa at strain of ~497.5% (Figure 2d). This tensile strength is higher than that of the nano-filler enhanced rubber[21] and comparable to that of recently published carbon dots enforced polymer matrix, whereas its healing efficiency is low.[22] In addition, the stress relaxation behavior was also measured for the $HDI_4PPG_1PY_3/Fe^{2+}$ complex with different molar ratio of Fe^{2+} and PY (Figure S9). In fact, the stress relaxation can be measured by two different methods. In the rheological shear test, the stress relaxation measurement is performed in the linear viscoelastic region, which detects the relaxation modulus under shear strain.[23] The stress relaxation of our experiment is tested by a tensile machine, which detects the tensile modulus under extensional strain.[24] In our case, the measurements were performed by stretching the samples to 50% strain and maintaining the strain for 30 min. The breaking and rebuilding of PY coordinated Fe^{2+} occur in the stretched PU/Fe^{2+} complex, thus allowing the network topologies of the elastomers to adapt to the applied forces. When the molar ratio of Fe^{2+}:PY is 1:6, the $HDI_4PPG_1PY_3/Fe^{2+}$ complex exhibits a slower stress relaxation rate compared to the complex with Fe^{2+}:PY at 1:4 and 1:8. This is reasonable for an elastomer with higher mechanical strength yielding a slower stress relaxation.[24b] Considering higher mechanical strength resulted by higher PY contents and appropriate metal ligand ratio, $HDI_4PPG_1PY_3/Fe^{2+}$ complex with metal ligand ratio of 1:6 was selected for the following mechanical and self-healing study.

The $HDI_4PPG_1PY_3/Fe^{2+}$ complex also exhibits the deformation-rate-dependent tensile behavior as shown in Figure 2e. A pronounced increase in both stress (from 2.3 MPa to 6.3 MPa) and Young's modulus (from 3.0 MPa to 4.4 MPa) is detected as the deformation rate increases from 50 mm/min to 500 mm/min. At the same time, the fracture strain of the complex is decreased (Figure 2f).This is a common phenomenon for most of the polymeric elastomers which is resulted from the hysteresis effect. At low deformation rate, the response is typical rubbery due to the dynamic and reversible metal-ligand-interactions; with increasing the deformation rate, resistance to polymer chain mobility causes stiffening in these materials.[25]

Therefore, the higher stress and modulus are observed at higher deformation rate in PU/Fe^{2+} complex.

To further investigate the mechanical properties of $HDI_4PPG_1PY_3/Fe^{2+}$ complex, 50 continuous cyclic tensile measurements were performed. As shown in Figure S10, the complex shows obvious hysteresis upon the first loading-unloading cycle at a strain of 250%, indicating the energy dissipation due to the coordination bond breakage during stretching. After 5 min waiting time, the second cycle was performed and showed that the tensional stress was lower than that in the first cycle. Correspondingly, the hysteresis loop with energy dissipation of 1.55 MJ/m^3 in the second cycle was smaller than that of 1.97 MJ/m^3 in the first cycle. The results indicate that the deformation of complex caused by tension cannot be completely recovered during the stretching process. However, after first five cycles, the hysteresis loops of the following 45 cycles reveal no much difference as shown in Figure 3a. This means

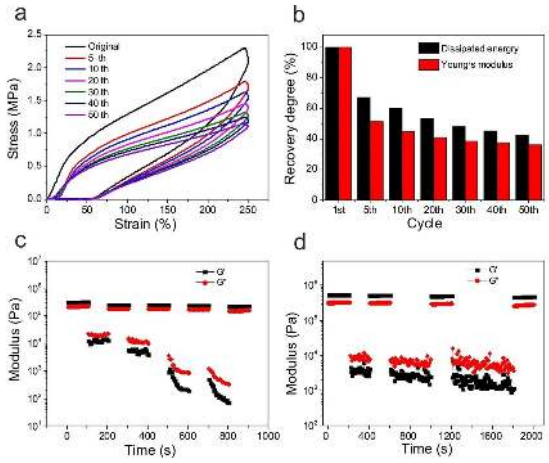

Figure 3. (a) Fifty continuous tensile loading and unloading cycles of $HDI_4PPG_1PY_3/Fe^{2+}$ complex at strain of 250%. A 5 min recovery time is introduced between each cycle. (b) Recovery degree of dissipated energy and Young's modulus for $HDI_4PPG_1PY_3/Fe^{2+}$ complex after 50 loading and unloading cycles. (c) G′ and G″ of the $HDI_4PPG_1PY_3/Fe^{2+}$ complex under alternate strain sweep at strain of 1, 100, 200, 400 and 600%, respectively. (d) G′ and G″ of the $HDI_4PPG_1PY_3/Fe^{2+}$ complex under alternate strain sweep with a small strain of 1% for 200 s, followed by a large strain of 200% for 200 s, 400 s and 600 s, respectively. Angular frequency is fixed at 10 rad/s.

that the molecular chain may slip to a certain extent after the first 5 cycles, then the whole network reaches a relatively stable state. In order to describe the recovery performance quantitatively, the stiffness recovery degree and toughness recovery degree were defined by calculating the ratios of Young's modulus and dissipated energy loss at different loading cycles to those values at the first one, respectively. As shown in Figure 3b, the $HDI_4PPG_1PY_3/Fe^{2+}$ complex can recover its stiffness by 51.2% and toughness by 67.3% after 5 cycles. Even after 50 cycles, stiffness and toughness recovery degrees can still remain at 36.2% and 42.3%, respectively, which demonstrates that $HDI_4PPG_1PY_3/Fe^{2+}$ complex possesses good recovery properties.

The $HDI_4PPG_1PY_3/Fe^{2+}$ complex not only possesses good toughness, high stiffness, and high strength, but also exhibits outstanding fatigue resistance properties. Therefore, we further checked the stress relaxation property of the complex, which is an important indicator of the fatigue resistant materials. As shown in Figure 3c, the $HDI_4PPG_1PY_3/Fe^{2+}$ complex was first treated by a small oscillatory shear strain of 1% and maintained for 100 s, G′ is slightly higher than G″. When the strain was increased from 1 to 100% and maintained for 100 s, G″ was increased to be higher than G′, and they immediately (less than 10 s) returned their original values once the strain was changed back to 1%. Similarly, G′ and G″ also quickly returned to the original values when we applied severe strain deformation (200, 400 and 600%) followed by small strain (1%). The dynamic alternate strain sweep measurements for different applying time (1% and 200%) were applied on the $HDI_4PPG_1PY_3/Fe^{2+}$ complex. As shown in Figure 3d, when the $HDI_4PPG_1PY_3/Fe^{2+}$ complex was treated by a 200% strain for different times, G′ immediately dropped and was lower than G″. When the strain was changed back to 1%, both G′ and G″ values could revert to the original values without any loss (Figure 3d). The nature of rapid recovered to the original state within a few seconds indicates the good fatigue resistance of the metal-coordinated complex.

In addition to these good mechanical properties, $HDI_4PPG_1PY_3/Fe^{2+}$ complex also exhibits super self-healing capacity under ambient conditions. Self-healing materials have been studied for decade and remarkable progresses have been made.[9a–g,10,11c,17a,26] However, most of these materials have an inherent compromise between mechanical strength and self-healing efficiency; the strong interactions usually lead to high mechanical strength and low healing efficiency, and healing process generally requires a certain amount of energy input, e.g., heat, light, or additives to induce healing; the weak interactions will make autonomous healing, but yield soft materials. In our case, the damaged $HDI_4PPG_1PY_3/Fe^{2+}$ soft elastomer can heal itself with high healing efficiency under ambient conditions. The self-healing behavior at the microscopic scale was first monitored using optical microscopy. As shown in Figure 4a–c, a scratch with 200 μm width could be filled by material diffusion at room temperature for 24 h. To further quantify the self-healing behavior, the healing efficiency of $HDI_4PPG_1PY_3/Fe^{2+}$ complex at different time was first studied. The rectangular complex film with 10 mm in width and 0.35 mm in thickness were then cut into halves and then healed by simple contact at room temperature for different periods of time. As shown in Figure 4d, the stress-strain curves of the healed samples basically coincide with that of the original one. Obviously, the healed complexes not only restored their Young's modulus but also restored the stress quickly, and their toughness increased quantitatively with time. After 6 h of contact, the healed sample recovered 42.2% of its initial stress. As healing time increases, the tensile strength increases. After 36 h the healed samples achieved 96.4% of their initial stress, indicating the complex was almost completely restored (Figure 4e). Further prolonging the healing time does not increase the tensile strength significantly. Interestingly, the healing

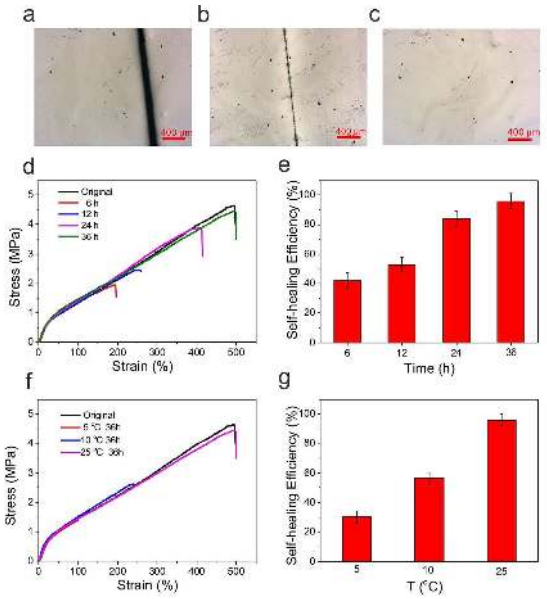

Figure 4. Self-healing properties of $HDI_4PPG_1PY_3/Fe^{2+}$ complex. Optical microscopy images of the complex film with about 200 μm damaged scar (a) and after healing at room temperature for 12 h (b) and 24 h (c), respectively. (d) Stress-strain curves of the original complex and healed complex by contacting two halves for different healing time at room temperature. (e) Self-healing efficiency of fracture stress of healed complexes for different healing time. (f) Stress-strain curves of original complex and healed complex after healing for 36 h at different temperatures. (g) Self-healing efficiency of fracture stress of healed complexes at different healing temperatures.

process can occur even at lower temperatures (Figure 4f). The stress-strain curves of the complexes healed at 10 °C and 5 °C coincide with that of original sample. Even at 5 °C, the healing efficiency is still at 30.2 % of its original stress (Figure 4g). The relatively low healing temperature and high healing efficiency may be due to the flexibility of the metal-coordinated PU caused by a low T_g (−5 °C), and the high coordination strength and high dynamics between PY and Fe^{2+}.

Previous self-healing systems utilizing metal-ligand interactions with larger terpyridine ligands required heat,[17a] UV light-converted local heat,[10] or solvent[11c] to induce healing. In our case, Fe^{2+} ions and PY ligand in the freshly cut interface interact with each other assisted by PU mobility, leading to the reconstruction of the network on the interface of the two halves. The observed healing behavior proves our assumption that introduction of a single pyridine-containing ligand with Fe^{2+} in the polyurethane matrix can lead to mechanical robustness and efficient self-healing. The healing efficiency of this metal-coordinated complex is even comparable to our previous reported hydrogel system,[27] but the complex has better mechanical properties. To further monitor the dynamic metal-ligand interaction in the system, the temperature-dependent sweeps were performed (Figure 5a). At the temperature of 25 °C and 45 °C, a large-amplitude sweep (200 % strain, 10 rad/s) can destroy the network structure, showing G′<G″. The followed small-amplitude sweep (1 % strain, 10 rad/s) leads to the fast recovery of the network (G′>G″). However, at high temperature of 75 °C, even at small-amplitude sweep (1 % strain,

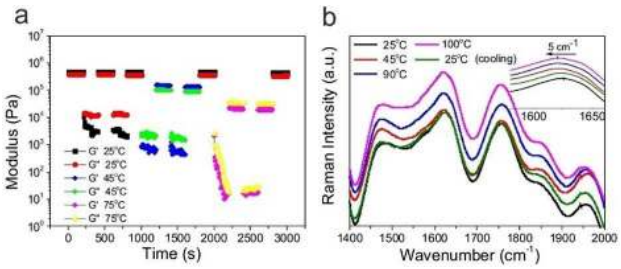

Figure 5. (a) G′ and G″ of the $HDI_4PPG_1PY_3/Fe^{2+}$ complex under alternate strain sweep between a small strain of 1 % and large strain of 200 % at different temperatures. The angular frequency is fixed at 10 rad/s. (b) Raman spectra of the $HDI_4PPG_1PY_3/Fe^{2+}$ complex at different temperatures. Inset: high resolution of the Raman spectra indicating the reversible coordinated-band shifts by heating the complex.

10 rad/s), the network was destroyed (G′<G″), indicating the disassociation of the metal-ligand interaction. When the temperature returned to room temperature, the network was re-established, showing that G′ is larger than G″ (Figure 5a). The in-situ Raman spectra of the solid complex further proves the temperature-dependent metal-ligand interaction. A variety of the molecular vibrations in the fingerprint region (1400–2000 cm^{-1}) indicates the association of the PY ligand with Fe^{2+}. As shown in the high resolution of the spectra (Figure 5b, inset), the peak of Fe^{2+}-PY at 1625 cm^{-1} shifts by 5 cm^{-1} upon heating the complex and recovers back to the original position upon cooling. These results are consistent with coordination of Fe^{2+} and PY monomer as confirmed by Raman spectra (Figure S11, S12). The heat-resulted reversible shift should be related to a structural rearrangement of the Fe^{2+}-PY complex, which is similar to the disassociation of the metal-ligand motifs caused by UV radiation converted heat.[28]

Despite the high mechanical strength and high self-healing capacity, a very surprising mechanical property of $HDI_4PPG_1PY_3/Fe^{2+}$ complex is notch-insensitivity. When the complex film was cut a notch and the notched complex film was stretched, the notch was relatively insensitive and stable, while the fracture usually occurred near the metal clamps (Figure 6a and movie S1). To quantitatively study the fracture energy of the notch-insensitive complex, we stretched the samples with different notch sizes at a constant rate of 100 mm/min. The fracture energy of the complex was determined using a method introduced by Rivlin and Thomas[29] and described in the experimental section in detail. The force-length curves of the unnotched and notched samples with different crack lengths were obtained (Figure 6b). When the notched samples are stretched, the deformation is inhomogeneous; the coordinated network directly ahead of the notch is stretched more than elsewhere. The critical stretches are identified when the notched samples show the crack propagation occurring during the stretching process. Different notch length results in different extent of crack propagation due to stress concentration. When the ratio of notch length to initial width is lower than 0.5, the stress concentration is not apparent and the critical stretches are almost unchanged (Figure S13). However, the fracture mechanism is a nonequilibrium process, developing

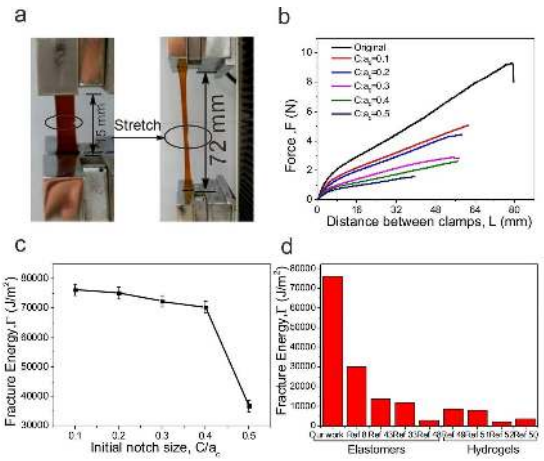

Figure 6. (a) Photographs of a notched sample under stretching. (b) Force-length curves for original sample and notched samples with various crack lengths (represented by C). (c) Fracture energy of notched samples with different C/a_0 ratios. (d) A comparison of $HDI_4PPG_1PY_3/Fe^{2+}$ complex to recent reported work in self-healing elastomers and hydrogels.

with time and involving consecutive rupture of the molecular chains.[30] When the notch length reaches to 50% of the whole complex film width, the unevenness of the stress per unit area of the notched sample increases, leading to a significant incision extension and resulting in rapid fracture of the sample. Therefore, the fracture energy as a function of crack lengths is calculated and shown in Figure 6c. As a result, a consistent fracture energy at 76186 J/m^2 within the range of $C/a_o < 0.4$ is obtained. This value is among the highest reported fracture energy values for self-healable polymers. For ease of comparison, the fracture energy of self-healing elastomers and tough hydrogels from the latest literatures listed in Table S1 and Table S2, are plotted in Figure 6d. Our $HDI_4PPG_1PY_3/Fe^{2+}$ complex demonstrates the extremely high fracture energy, far beyond the healable elastomers[5a,14,31,32] and tough hydrogel.[33] Usually, the stable crack propagation is found in nanoplatelets reinforced materials and nacre-mimetic nanocomposites.[34] In this work, the notch-insensitive behavior of the metal-coordinated complex in sharp contrasts to the stiff and brittle nanocomposites and displays that multiple metal-ligand interactions facilitate energy dissipation, while stiffening and toughing the mechanical properties of the materials and maintaining crack stability. The high fracture energy value is probably due to the efficient energy dissipation arising from the association and disassociation of the metal-ligand interaction in the system.

From the above discussion, it can be seen that our $HDI_4PPG_1PY_3/Fe^{2+}$ complex not only possesses multiple good mechanical properties, including high stiffness, high strength, good toughness, and fatigue resistance as well as notch-insensitivity, but also possesses good healing capacity under ambient condition without any external stimuli. To further illustrate the critical role of Fe^{2+}-PY coordination in the system, a more detailed analysis was carried out. Firstly, considering the instability of Fe^{2+} and its ease of oxidation into Fe^{3+}, X-ray photoelectron spectroscopy measurement for $HDI_4PPG_1PY_3/Fe^{2+}$ complex was conducted (Figure S14). The multiplet peaks coincide with the peaks in high-resolution Fe^{2+} $2P_{3/2}$ spectra indicating that the metal ion preserves Fe^{2+} state.[35]

Secondly, the bonding configurations of Fe^{2+}-PY coordination should play a key role in the process of self-healing. The coordination geometry between Fe^{2+} and PY ligand is typically octahedral, where Fe^{2+} is hexahedral, as confirmed by UV-Vis spectroscopy (Figure S2), similar to the coordination between Fe^{2+} and bipyridine.[36] Due to a mono-coordination site of PY, the coordination geometry between Fe^{2+} and PY can be matched in different configurations. Upon loading on the complex, penta or tetrahedral-coordinated Fe^{2+} complex will be formed, which is meta-stable.[37] The meta-stable state can be maintained for certain time but not completely disassociated. Because PY ligands are distributed throughout the whole network and ease to move due to low T_g of the complex, a free PY ligand is easy to appear around the meta-stable complex. Thus, the penta or tetrahedral-coordinated Fe^{2+} complex will combine the free PY ligands to reform a stable hexahedral-coordinated Fe^{2+} complex (Figure 1b). Meanwhile, in the process of chain unfolding and sliding the dynamic disassociation and reconstruction of the Fe^{2+}-PY coordination will dissipate energy and realize self-healing.

Thirdly, a high bonding strength of Fe^{2+}-PY is responsible for the high mechanical strength. To further prove this, a new complex coordinated by Zn^{2+} instead of Fe^{2+} was fabricated (Figure S15). The $HDI_4PPG_1PY_3/Zn^{2+}$ complex exhibits weak mechanical strength compared to the $HDI_4PPG_1PY_3/Fe^{2+}$ complex, which is mainly due to the weaker binding strength and more kinetic instability of Zn^{2+}-PY.[17b] If the binding strength of the complex is too high we also see no self-healing.[17a] This is in agreement with the current work that the coordination structure of the metal and ligand play a crucial role in determining the rigidity vs. mobility in these polymer networks.

Fourthly, instead of PY ligand, a control monomer (benzene-containing diol, BE) with similar structure to PY was synthesized to further confirm the role of PY ligand (see supporting information, Scheme S2, Figure S16). The control PU_2 ($HDI_4PPG_1BE_3$) was obtained by using the same molar ratio monomer to $HDI_4PPG_1PY_3$ and indicates sticky gel-like state (Figure S17a). After addition of $FeSO_4$, the control PU_2/Fe^{2+} complex with Fe^{2+} to BE ratio of 1:6 still cannot form free-standing films (Figure S17b). Although the modulus increases compared to that of pristine PU_2 due to the weak metal-ligand interaction between amide in the PU_2 structure and Fe^{2+}, the control complex still behave soft state ($G' < G''$). Therefore, PY ligands are the critical for the mechanical strength of $HDI_4PPG_1PY_3/Fe^{2+}$ complex.

Conclusion

We have developed a series of metal-coordinated complexes by introducing a mono-pyridine-containing ligand into PU. The complexes with different molar ratio of Fe^{2+} and PY were studied. By optimizing the monomer ratio and Fe^{2+} content, the $HDI_4PPG_1PY_3/Fe^{2+}$ complex with Fe^{2+} to PY ratio of 1:6

possesses multiple good mechanical properties, including high tensile strength (up to 4.64 MPa), high Young's modulus (3.2 MPa), and high elongation (~497.5%) at strain rate of 100 mm/min as well as fatigue resistance. Importantly, the metal-complex exhibits outstanding healing efficiency of ~96% of tensile strength at room temperature and ~30% at low temperature of 5 °C. The dynamic and reversible metal-ligand interactions in the solid state can dissipate energy and should be responsible for the good mechanical performance and self-healing ability. More importantly, the complex is notch-insensitive and the fracture energy is ~76186 J/m^2, which is among the highest values for the reported self-healing polymeric materials. Our work provides a new strategy for fabricating materials with high mechanical properties and high self-healing ability.

Experimental Section

Materials

2-(chloromethyl)pyridine hydrochloride (98%), diethanolamine, hexamethylene diisocyanate (HDI), poly(propylene glycol) (PPG, M_n = 400 and 1000 g/mol), iron sulfate heptahydrate ($FeSO_4 \cdot 7H_2O \geq$ 99%) were supplied by Aladdin. Sodium carbonate anhydrous, methanol anhydrous, acetone, magnesium sulfate anhydrous were received from Sinopharm Chemical Reagent Beijing Co. Ltd. Beijing, China. Isopropanol and dichloromethane was obtained from Fuyu Fine Chemical Co. Ltd. Tianjin, China. All other reagents (analytical grade) were used directly without further purification.

N-(2-Pyridylmethyl)iminodiethanol (PY)

The ligand PY was fabricated through modifying a previously reported method.[18] Typically, Diethanolamine (6.41 g), 2-(chloromethyl)pyridine hydrochloride (10.0 g) and sodium carbonate (19.38 g) were dissolved in isopropanol and the solution was refluxed overnight. After isopropanol was evaporated, the solid was extracted with dichloromethane and saturated brine. The dichloromethane solution was collected and dried by magnesium sulfate anhydrous. After dichloromethane was removed, the resulting PY was obtained (yield 45%): ^{1}H NMR in D_2O, 400 MHz, 2.66 (t, 4H, NCH_2CH_2), 3.61 (t, 4H, CH_2OH), 3.77 (s, 2H, $PyCH_2N$), 7.40, 7.44, 7.81, 8.40 (td, dd, td, dd, 4 H, pyridine H) (Figure S1). Elemental analysis calculated for $C_{10}H_{16}N_2O_2$: C, 61.20; H, 8.22; N, 14.27. Found: C, 61.15; H, 8.25; N, 14.23.

Synthesis of Polyurethanes (PUs)

During the polyurethane synthesis, different diols will be used, which will be related to the hard and soft segments of the polyurethane. In our case, we selected small molecular PY as the chain extender. PY can be well dissolved into acetone solvent and no clustering of the ligands is observed during PU synthesis. Typically, HDI (3.0 g, 17.8 mmol) and PPG400 (1.78 g, 4.4 mmol) were added in a dried glass vessel and were heated in an oil bath with stirring at 100 °C under a N_2 atmosphere for 1.5–2 h. After the synthesis of the pre-polymer, PY (2.63 g, 13.4 mmol) as a chain extender and acetone as solvent were added to the reactor. The reaction was reheated to 100 °C under a N_2 atmosphere for 12 h until the NCO groups disappeared. The resulting PUs were obtained by pouring the solution into a Teflon mold for drying at 80 °C for 24 h. Different PUs can be obtained by changing the segment ratio of HDI, PPG and PY. Different PUs can be synthesized by changing the molar ratio of HDI, PPG and PY.

Metal-Coordinated PU Complex

The dried PU with different PY content and a certain amount of $FeSO_4.7H_2O$ were dissolved in methanol with stirring for 15 min followed by ultrasound for 20 min. Then, the solution was allowed to stand for 10 min. The complex solution was then poured into a Teflon mold for drying at 35 °C for 10 h. The final complex was obtained by further removing solvent residue in a 70 °C vacuum oven over 2 days. Different metal-coordinated complexes can be obtained by tuning the ratio of Fe^{2+} and PY.

Mechanical Testing

A universal test instrument (Hensgrand, WDW-02, China) was used to measure mechanical properties. The metal-coordinated complex films with 10 mm width, 0.35 mm thickness were measured at different strain rate at room temperature. By using the Equation (1), the tensile stress (σ) was measured.

$$\sigma = F/a_0 b_0 \quad (1)$$

where F represents the load and a_0 represents the width, b_0 represents thickness of the specimen.

The tensile strain (ε) was determined by following Equation (2):

$$\varepsilon = (l\text{-}l_0)/l_0 \times 100\,\% \quad (2)$$

where l_0 is the initial gauge length and l is the tensile length of the specimen. The Young's modulus was determined as the slope of the stress-strain curve in the first 20% strain.

The complex films with the same size (10 mm width and 0.35 mm thickness) were used to measure cyclic tensile tests at the rate of 100 mm/min. At least three specimens were tested. The dissipated energy (ΔU) of the complex film for each cycle is calculated by integrating the area surrounded by the loading and unloading curves [Eq. (3)]:

$$\Delta U = \int_{\text{loading}} \sigma \, d\varepsilon - \int_{\text{unloading}} \sigma \, d\varepsilon \quad (3)$$

Dynamic viscoelasticity of the complex films were measured on a rheometer (TA DHR-2) using a parallel plate of 20 mm diameter. The linear viscoelasticity region was determined by the dynamic strain sweep with a constant frequency of 10 rad/s in the range of 0.1 ~ 100%. The frequency sweep of the complex film was recorded at a fixed strain of 1% over the frequency range of 0.1 ~ 100 rad/s. The alternate step strain (1, 100, 200, 400 and 600%) sweep of the complex film was recorded at a constant angular frequency of 10 rad/s. The temperature was controlled by a Peltier plate.

Determination of Fracture Energy

The fracture energy of the complex films was determined by in tension mode. Firstly, the force-length curve was recorded by an unnotched specimen. The work done (W(L)) by the force to the unnotched specimen is determined by integrating the area under the force-length curve. Then, different specimens of the same complex were notched with different crack length (C). The notched

specimens were stretched until the notch turned into a running crack to determine the critical length (*Lc*). Fracture energy was determined as $\Gamma=\frac{W(L_c)}{a_0 b_0}$, where Γ represents the fracture energy, a_0 represents the sample width, b_0 represents the sample thickness.

Self-healing Process

The metal-coordinated complex film was cut into two halves. Then the two halves were contacted with each other in air at room temperature for different times. The healed samples were measured in tensile mode at a rate of 100 mm/min. For healing at low temperature, the contacted pieces were put in refrigerator and held at 10 °C or 5 °C for 36 h.

Characterizations

^{1}H NMR spectra were recorded with a ^{1}H NMR spectrometer (Bruker AVANCE II 400).UV-vis absorption spectra were measured on a UV-2600 UV-vis spectrometer (Shimadzu, Japan). Differential scanning calorimetry (DSC) was performed using a TAQ-10 DSC instrument. The experiments were conducted in heating-cooling-heating cycles and the data were obtained during the second heating cycle with a heating rate of 10 °C/min from −70 °C to 150 °C. Raman spectra were recorded using a LabRAM tHR800 Raman spectrometer (HORIBA JY, France). An excitation wavelength of 633 nm was used. X-ray photoelectron spectroscopy (XPS) measurements were taken in an ESCALAB 250 (Thermo Fisher Scientific, USA) using a monochromatic Al–Kα X-ray source at 100 W.

Acknowledgements

This work was supported by Research Leader Foundation of "20 Policies of Colleges and Universities" of Jinan City (2018GXRC027), the National Key Research and Development Program of China (2017YFA0206901, 2017YFA0206900), the National Natural Science Foundation of China (21705027), the Natural Science Foundation of Shandong Province (ZR2017MB009, ZR2017BEM020, ZR2017LEM010) and Young Doctoral Cooperation Fund of Qilu University of Technology (Shandong Academy of Sciences) (2017BSHZ014), the Natural Science Foundation of Shanghai, and the Recruitment Program of Global Experts of China and the Thousand Talent Plan of Shanghai.

Conflict of interest

The authors declare no conflict of interest.

Keywords: elastomers · metal coordination · notch-insensitivity · polyurethane self-healing

[1] a) D. Döhler, P. Michael, W. H. Binder, *Acc. Chem. Res.* **2017**, *50*, 2610–2620; b) C. S. Luo, P. Wan, H. Yang, S. A. A. Shah, X. Chen, *Adv. Funct. Mater.* **2017**, *27*, 1606339; c) T. P. Huynh, P. Sonar, H. Haick, *Adv. Mater.* **2017**, *29*, 1604973; d) R. P. Wool, *Soft Matter* **2008**, *4*, 400–418.

[2] R. C. R. Gergely, W. A. S. Cruz, B. P. Krull, E. L. Pruitt, J. Wang, N. R. Sottos, S. R. White, *Adv. Funct. Mater.* **2018**, *28*, 1704197.

[3] a) H. Ying, Y. Zhang, J. Cheng, *Nat. Commun.* **2014**, *5*, 3218; b) W. Zou, J. Dong, Y. Luo, Z. Qian, X. Tao, *Adv. Mater.* **2017**, *29*, 1606100.

[4] T. J. Cuthbert, J. J. Jadischke, J. R. D. Bruyn, P. J. Ragogna, E. R. Gillies, *Macromolecules* **2017**.

[5] a) X. Yan, Z. Liu, Q. Zhang, J. Lopez, H. Wang, H. C. Wu, S. Niu, H. Yan, S. Wang, T. Lei, *J. Am. Chem. Soc.* **2018**, *140*, 5280–5289; b) D. Clarke, E. T. Pashuck, S. Bertazzo, J. V. M. Weaver, M. M. Stevens, *J. Am. Chem. Soc.* **2017**, *139*, 7250–7255; c) B. Zhu, N. Jasinski, A. Benitez, M. Noack, D. Park, A. S. Goldmann, A. Walther, *Angew. Chem. Int. Ed.*, **2015**, *127*, 8777–8781.

[6] S. Burattini, B. W. Greenland, D. H. Merino, W. Weng, J. Seppala, H. M. Colquhoun, W. Hayes, M. E. Mackay, I. W. Hamley, S. J. Rowan, *J. Am. Chem. Soc.* **2010**, *132*, 12051–12058.

[7] a) K. Miyamae, M. Nakahata, Y. Takashima, A. Harada, *Angew. Chem. Int. Ed.* **2015**, *54*, 8984–8987; *Angew. Chem.* **2015**, *127*, 9112–9115; b) T. Kakuta, Y. Takashima, M. Nakahata, M. Otsubo, H. Yamaguchi, A. Harada, *Adv. Mater.* **2013**, *25*, 2849–2853; c) M. Zhang, D. Xu, X. Yan, J. Chen, S. Dong, B. Zheng, F. Huang, *Angew. Chem. Int. Ed.* **2012**, *51*, 7011–7013; *Angew. Chem.* **2012**, *124*, 7117–7121.

[8] a) G. R. Whittell, M. D. Hager, U. S. Schubert, I. Manners, *Nat. Mater.* **2011**, *10*, 176–188; b) J. Uchida, M. Yoshio, S. Sato, H. Yokoyama, M. Fujita, T. Kato, *Angew. Chem. Int. Ed.* **2017**, *56*, 14085–14089; *Angew. Chem.* **2017**, *129*, 14273–14277.

[9] a) Z. Wei, J. H. Yang, J. Zhou, F. Xu, M. Zrínyi, P. H. Dussault, Y. Osada, Y. M. Chen, *Chem. Soc. Rev.* **2014**, *43*, 8114–8131; b) N. N. Xia, X. M. Xiong, J. Wang, M. Z. Rong, M. Q. Zhang, *Chem. Sci.* **2016**, *7*, 2736–2742; c) R. J. Wojtecki, M. A. Meador, S. J. Rowan, *Nat. Mater.* **2011**, *10*, 14–27; d) N. Holtenandersen, M. J. Harrington, H. Birkedal, B. P. Lee, P. B. Messersmith, K. Y. Lee, J. H. Waite, *Proc. Natl. Acad. Sci. USA* **2011**, *108*, 2651–2655; e) S. Theis, A. Iturmendi, C. Gorsche, M. Orthofer, M. Lunzer, S. Baudis, A. Ovsianikov, R. Liska, U. Monkowius, I. Teasdale, *Angew. Chem. Int. Ed.* **2017**, *56*, 15857–15860; *Angew. Chem.* **2017**, *129*, 16071–16075; f) P. S. Yavvari, A. Srivastava, *J. Mater. Chem. B* **2015**, *3*, 899–910; g) H. P. Cong, P. Wang, S. H. Yu, *Chem. Mater.* **2013**, *25*, 3357–3362; h) M. Enke, R. K. Bose, S. Bode, J. Vitz, F. H. Schacher, S. J. Garcia, S. van der Zwaag, M. D. Hager, U. S. Schubert, *Macromolecules* **2016**, *49*, 8418–8429; i) S. Bode, M. Enke, R. K. Bose, F. H. Schacher, S. J. Garcia, S. van der Zwaag, M. D. Hager, U. S. Schubert, *J. Mater. Chem. A* **2015**, *3*, 22145–22153.

[10] M. Burnworth, L. Tang, J. R. Kumpfer, A. J. Duncan, F. L. Beyer, G. L. Fiore, S. J. Rowan, C. Weder, *Nature* **2011**, *472*, 334.

[11] a) Yuan, Jinchun, Fang, Xiuli, Zhang, Lingxing, Hong, Guangning, Lin, Yangju, *J. Mater. Chem.* **2012**, *22*, 11515–11522; b) B. Yang, H. Zhang, H. Peng, Y. Xu, B. Wu, W. Weng, L. Li, *Polym. Chem.* **2014**, *5*, 1945–1953; c) G. Hong, H. Zhang, Y. Lin, Y. Chen, Y. Xu, W. Weng, H. Xia, *Macromolecules* **2013**, *46*, 8649–8656.

[12] Q. Zheng, Z. Ma, S. Gong, *J. Mater. Chem. A* **2016**, *4*, 3324–3334.

[13] Y. L. Rao, A. Chortos, R. Pfattner, F. Lissel, Y. C. Chiu, V. Feig, X. Jie, T. Kurosawa, X. Gu, W. Chao, *J. Am. Chem. Soc.* **2016**, *138*, 6020–6027.

[14] J. Kang, D. Son, G. N. Wang, Y. Liu, J. Lopez, Y. Kim, J. Y. Oh, T. Katsumata, J. Mun, Y. Lee, *Adv. Mater.* **2018**, *30*, 1706846.

[15] C. H. Li, C. Wang, C. Keplinger, J. L. Zuo, L. Jin, Y. Sun, P. Zheng, Y. Cao, F. Lissel, C. Linder, *Nat. Chem.* **2016**, *8*, 618–624.

[16] D. Mozhdehi, S. Ayala, O. R. Cromwell, Z. Guan, *J. Am. Chem. Soc.* **2014**, *136*, 16128–16131.

[17] a) S. Bode, L. Zedler, F. H. Schacher, B. Dietzek, M. Schmitt, J. Popp, M. D. Hager, U. S. Schubert, *Adv. Mater.* **2013**, *25*, 1634–1638; b) Y. L. Rao, A. Chortos, R. Pfattner, F. Lissel, Y. C. Chiu, V. Feig, J. Xu, T. Kurosawa, X. Gu, C. Wang, *J. Am. Chem. Soc.* **2016**, *138*, 6020–6027.

[18] D. C. Crans, A. D. Keramidas, S. S. Amin, O. P. Anderson, S. M. Miller, *J. Chem. Soc. Dalton Trans.* **1997**, 2799–2812.

[19] Y. Liang, D. Strohecker, V. Lynch, B. J. Holliday, R. A. Jones, *ACS Appl. Mater. Interfaces* **2016**, *8*, 34568–34580.

[20] S. Coulibaly, A. Roulin, S. Balog, M. V. Biyani, E. J. Foster, S. J. Rowan, G. L. Fiore, C. Weder, *Macromolecules* **2014**, *47*, 152–160.

[21] a) C. Xu, L. Cao, X. Huang, Y. Chen, B. Lin, L. Fu, *ACS Appl. Mater. Interfaces* **2017**, *9*, 29363–29373; b) S. I. S. Shahabadi, J. Kong, X. Lu, *ACS Sustainable Chem. Eng.* **2017**, *5*, 3148–3157.

[22] C. Zhu, Y. Fu, C. Liu, Y. Liu, L. Hu, J. Liu, I. Bello, H. Li, N. Liu, S. Guo, *Adv. Mater.* **2017**, *29*, 1701399.

[23] N. Phan-Thien, M. J. J. O. N.-N. F. M. Safari-Ardi **1998**, *74*, 137–150.

[24] a) Z. Tang, J. Huang, B. Guo, L. Zhang, F. Liu, *Macromolecules* **2016**, *49*, 1781–1789; b) C. Bao, Y. J. Jiang, H. Zhang, X. Lu, J. Sun, *Adv. Funct. Mater.* **2018**, *28*, 1800560.

[25] C. R. Siviour, J. L. Jordan, *Journal of Dynamic Behavior of Materials* **2016**, *2*, 15–32.

[26] Y. Yang, M. W. Urban, *Chem. Soc. Rev.* **2013**, *42*, 7446–7467.

[27] C. Pan, L. Liu, Q. Chen, Q. Zhang, G. Guo, *ACS Appl. Mater. Interfaces* **2017**, *9*, 38052–38061.
[28] S. Coulibaly, A. Roulin, S. Balog, M. V. Biyani, E. J. Foster, S. J. Rowan, G. L. Fiore, C. Weder, *Macromolecules* **2013**, *47*, 152–160.
[29] R. S. Rivlin, A. G. Thomas, *J. Polym. Sci.* **1953**, *10*, 291–318.
[30] a) Young, J. Robert, *Fracture behaviour of polymers*, **1983**. b) S. Jeong-Yun, Z. Xuanhe, W. R. K. Illeperuma, C. Ovijit, O. Kyu Hwan, D. J. Mooney, J. J. Vlassak, S. Zhigang, *Nature* **2012**, *489*, 133–136.
[31] L. Cai, J. Wu, D. Weitz, *Adv. Mater.* **2017**, *29*, 1702616.
[32] E. M. Foster, E. E. Lensmeyer, B. Zhang, P. Chakma, J. A. Flum, J. J. Via, J. L. Sparks, D. Konkolewicz, *ACS Macro Lett.* **2017**, *6*, 495–499..
[33] a) J. Y. Sun, X. Zhao, W. R. Illeperuma, O. Chaudhuri, K. H. Oh, D. J. Mooney, J. J. Vlassak, Z. Suo, *Nature* **2012**, *489*, 133–136; b) T. L. Sun, T. Kurokawa, S. Kuroda, A. B. Ihsan, T. Akasaki, K. Sato, M. A. Haque, T. Nakajima, J. P. Gong, *Nat. Mater.* **2013**, *12*, 932–937; c) H. Chen, Y. Liu, B. Ren, Y. Zhang, J. Ma, L. Xu, Q. Chen, J. Zheng, *Adv. Funct. Mater.* **2017**, *27*, 1703086; d) H. Jia, Z. Huang, Z. Fei, P. J. Dyson, Z. Zheng, X. Wang, *ACS Appl. Mater. Interfaces* **2016**, *8*, 31339–31347.
[34] a) T. Verho, M. Karesoja, P. Das, L. Martikainen, R. Lund, A. Alegría, A. Walther, O. Ikkala, *Adv. Mater.* **2013**, *25*, 5055–5059; b) B. Zhu, N. Jasinski, A. Benitez, M. Noack, D. Park, A. S. Goldmann, C. Barner-Kowollik, A. Walther, *Angew. Chem. Int. Ed.* **2015**, 54, 8653–8657; *Angew. Chem.* **2015**, *127*, 8777–8781.
[35] A. P. Grosvenor, B. A. Kobe, M. C. Biesinger, N. S. Mcintyre, *Surf. Interface Anal.* **2004**, *36*, 1564–1574.
[36] D. E. Przybyla, J. Chmielewski, *J. Am. Chem. Soc.* **2010**, *132*, 7866–7867.
[37] B. Weber, E.-G. Jäger, *Eur. J. Inorg. Chem.* **2009**, 465–477.

Manuscript received: February 6, 2019
Revised manuscript received: April 2, 2019
Accepted manuscript online: April 4, 2019